

Supporting Information for the manuscript:

Dicopper(II) Metallacyclophanes Featuring Acridine-Based Spacers: Long-Range Magnetic Coupling and Selective Catalytic Oxidation of Hydroquinone

Lucas Hoffmann Greghi Kalinke,^a Maria Clara Orioli Emidio Souza,^b Pedro Victor Valadares Romanholo,^b Jackson Junior Santos de Souza,^b Antonio Carlos Roveda Jr.,^c Sergio Antonio Spinola Machado,^c Ana Karoline Silva Mendanha Valdo,^d Felipe Terra Martins,^b Renato Rabelo,^{b,e} Joan Cano,^{e,} Francesc Lloret,^e Miguel Julve,^e Livia Florio Sgobbi,^{b,*} Danielle Cangussu^{b,*}*

^a*Instituto Federal de Goiás, Campus Anápolis, Anápolis, GO, 75131-457, Brazil.*

^b*Instituto de Química, Universidade Federal de Goiás, Goiânia, Goiás, 74690-900, Brazil. E-mail: danielle_cangussu@ufg.br; livia_sgobbi@ufg.br.*

^c*Instituto de Química de São Carlos, Universidade de São Paulo, São Carlos, São Paulo, 13566-590, Brazil.*

^d*Instituto Federal Goiano, IF Goiano – Campus Iporá, Iporá, Goiás, 74200-264, Brazil.*

^e*Departament de Química Inorgànica/Instituto de Ciencia Molecular (ICMol), C/ Catedrático José Beltrán 2, 46980 Paterna (Valencia), Spain. E-mail: joan.cano@uv.es.*

List of Contents:

Crystallographic data of **1** and **2** (Tables S1–S5);

XPRD patterns of **1** (Figure S1);

FT-IR spectra of **1** and **2** (Figure S2);

UV-Vis spectra of **1** and **2** (Figures S3 and S4);

Detailed structure views of **1** and **2** (Figures S5–S7);

Catalytic activity of **1** and **3** (Figures S8–S10)

Magnetic properties of **2** (Figure S11)

Spin Density Maps (Figures S12–S16)

Table S1. Crystal data and refinement parameters for compounds **1** and **2**

Chemical Formula	$C_{34}H_{42}Cu_2N_6Na_4O_{26}$	
M (g mol ⁻¹)	1169.78	
Crystal system	Monoclinic	
Space group	$P2_1$	
Z	2	
Unit cell dimensions	a (Å) 16.306(3) b (Å) 7.5244(13) c (Å) 18.238(4) α (°) 90 β (°) 98.206(8) γ (°) 90	
V (Å ³)	2214.7(7)	
ρ_{calc} (g cm ⁻³)	1.754	
μ (mm ⁻¹)	1.102	
T (K)	298	
θ range for data collection (°)	1.809–25.040	
h	−19 to 19	
k	−8 to 8	
l	−21 to 21	
Data collected/Unique reflections/ $I > 2\sigma(I)$	22219/7831/4243	
Symmetry factor (R_{int})	0.1782	
Completeness to θ_{max} (%)	99.6	
$F(000)$	1196	
Refined parameters	652	
Goodness-of-fit on F^2 (S)	0.998	
Final R_I factor ^a [$I > 2\sigma(I)$]	0.0783	
wR_2 factor ^b (all data)	0.1938	
Largest diff. peak/hole ($e \text{ Å}^{-3}$)	1.410/−0.893	
CCDC deposit no.	2083644	
^a $R_I = \sum(F_o - F_c)/\sum F_o $. ^b $wR_2 = [\sum w(F_o^2 - F_c^2)^2/\sum w(F_o^2)^2]^{1/2}$.		

Table S2. Bond lengths (Å) and angles (deg) for **1**.

Bond	Length	Bond	Length	Bond	Angle	Bond	Angle
Cu1—N6	1.950(14)	Na4—O2 ⁱⁱ	2.365(14)	O9—Na1—O6W ^v	87.3(6)	O4W—Na3—O5W	84.8(8)
Cu1—N3	1.975(12)	Na4—O7W	2.436(2)	O3—Na1—O9	67.4(4)	O10—Na3—O5W	158.2(8)
Cu1—O12	1.970 (13)	Na4—O10W	2.405(3)	O11 ^v —Na1—O1W	102.0(5)	O11 ⁱ —Na3—O6W	88.5(7)
Cu1—O6	1.963(14)	Na4—O13W*	2.127(4)	O1W—Na1—O6W ^v	88.4(6)	O11 ⁱ —Na3—O4W	82.6(7)
Cu1—O11W	2.728(3)	Na4—O14W*	2.268(5)	O3—Na1—O1W	79.6(4)	O11 ⁱ —Na3—O10	105.5(6)
Cu2—N1	1.988(12)	Bond	Angle	O9—Na1—O1W	83.9(4)	O11 ⁱ —Na3—O5W	92.6(7)
Cu2—N4	1.933(13)	N3—Cu1—N6	108.0(5)	O11 ^v —Na1—O2W	91.8(5)	O11—Na3—O6W	77.2(7)
Cu2—O3	1.947(11)	N3—Cu1—O6	83.9(5)	O2W—Na1—O6W ^v	106.6(7)	O11—Na3—O4W	115.5(7)
Cu2—O9	2.004(11)	N3—Cu1—O12	163.9(5)	O3—Na1—O2W	82.0(5)	O10—Na3—O11	65.5(5)
Cu2—O3W	2.364(9)	N3—Cu1—O11W	96.4(6)	O9—Na1—O2W	85.5(5)	O11—Na3—O5W	101.4(7)
Na1—O3	2.400(12)	N6—Cu1—O6	168.1(6)	O1W—Na1—O2W	161.2(5)	O11—Na3—O11 ⁱ	157.8(6)
Na1—O9	2.386(12)	N6—Cu1—O12	83.1(6)	O1W ^{iv} —Na2—O3W	116.3(4)	O6—Na4—O13W*	87.3(11)
Na1—O11v	2.355(12)	N6—Cu1—O11W	91.3(6)	O8—Na2—O3W	148.6(5)	O6—Na4—O14W*	85.0(14)
Na1—O6W ^v	2.419(3)	O6—Cu1—O12	85.1(6)	O8—Na2—O1W ^{iv}	93.5(4)	O2 ⁱⁱ —Na4—O13W*	108.0(10)
Na1—O1W	2.384(12)	O6—Cu1—O11W	88.1(6)	O7—Na2—O3W	78.2(4)	O2 ⁱⁱ —Na4—O14W*	112.0(14)
Na1—O2W	2.451 (16)	O12—Cu1—O11W	95.0(6)	O7—Na2—O1W ^{iv}	153.6(5)	O2 ⁱⁱ —Na4—O6	163.0(6)
Na2—N5 ⁱⁱⁱ	2.758 (13)	N1—Cu2—N4	107.7(5)	O7—Na2—O8	70.5(4)	O7W—Na4—O13W*	102.3(11)
Na2—O3 ^{iv}	2.554 (11)	N1—Cu2—O3	83.5(5)	O3 ^{iv} —Na2—O3W	77.6(4)	O7W—Na4—O14W*	77.8(13)
Na2—O7	2.387(13)	N1—Cu2—O9	157.4(5)	O3 ^{iv} —Na2—O1W ^{iv}	76.3(4)	O6—Na4—O7W	85.8(6)
Na2—O8	2.378(13)	N1—Cu2—O3W	110.0(4)	O3 ^{iv} —Na2—O8	101.7(4)	O2 ⁱⁱ —Na4—O7W	97.8(6)

Na2—O3W	2.360(12)	N4—Cu2—O3	166.5(5)	O3 ^{iv} —Na2—O7	86.3(4)	O10W—Na4—O13W*	60.3 (10)
Na2—O1W ^{iv}	2.402(14)	N4—Cu2—O9	82.4(5)	N5 ⁱⁱⁱ —Na2—O3W	96.8(4)	O10W—Na4—O14W*	84.8(14)
Na3—O10	2.372(15)	N4—Cu2—O3W	92.3(4)	N5 ⁱⁱⁱ —Na2—O1W ^{iv}	88.9(4)	O6—Na4—O10W	96.2(6)
Na3—O11	2.666(19)	O3—Cu2—O9	84.5(4)	N5 ⁱⁱⁱ —Na2—O8	93.4(4)	O2 ⁱⁱ —Na4—O10W	85.5(6)
Na3—O11 ⁱ	2.570(19)	O3—Cu2—O3W	90.8(4)	N5 ⁱⁱⁱ —Na2—O7	112.2(4)	O7W—Na4—O10W	162.2(8)
Na3—O4W	2.318(2)	O9—Cu2—O3W	89.2(4)	N5 ⁱⁱⁱ —Na2—O3 ^{vi}	159.3(4)	O12—Na4—O13W*	147.4(14)
Na3—O5W	2.374(2)	O11 ^v —Na1—O6W ^v	80.8(6)	O4W—Na3—O6W	162.4(9)	O12—Na4—O14W*	149.3(17)
Na3—O6W	2.273(3)	O3—Na1—O11 ^v	125.4(5)	O10—Na3—O6W	111.5(8)	O6—Na4—O12	64.8(5)
Na4—O6	2.314(14)	O3—Na1—O6W ^v	152.8(6)	O10—Na3—O4W	85.6(7)	O2 ⁱⁱ —Na4—O12	98.3(5)
Na4—O12	2.623(18)	O9—Na1—O11 ^v	166.5(5)	O5W—Na3—O6W	80.5(8)	O12—Na4—O7W	93.7(6)
						O12—Na4—O10W	103.2(7)

Symmetry codes (the same ones used in Figure 1): (i) $-x, \frac{1}{2}+y, 1-z$; (ii) $x, y, -1+z$; (iii) $-x, \frac{1}{2}+y, 2-z$; (iv) $x, 1+y, z$; (v) $x, y, 1+z$. *O13W and O14W belong to the same disordered water molecule and are in 60% and 40% occupancy sites, respectively.

Table S3. Bond lengths (\AA) and angles (deg) for 2.

Bond	Length	Bond	Angle
Cu1—N1	1.948(8)	N1—Cu1—N4	109.0(3)
Cu1—N4	1.966(6)	N1—Cu1—O1	83.5(3)
Cu1—O1	1.934(6)	N1—Cu1—O7	163.7(3)
Cu1—O7	1.923(8)	N4—Cu1—O1	164.1(3)
Cu2—N3	1.941(7)	N4—Cu1—O7	83.6(3)
Cu2—N6	1.943(8)	O1—Cu1—O7	86.2(3)
Cu2—O6	1.945(8)	N3—Cu2—N6	108.1(3)
Cu2—O12	1.918(7)	N3—Cu2—O6	83.0(3)
		N3—Cu2—O12	166.5(3)
		N6—Cu2—O6	166.7(3)
		N6—Cu2—O12	84.2(3)
		O6—Cu2—O12	85.6(3)

Table S4. Hydrogen bonds in the crystal structure of **1** (D and A are abbreviations for hydrogen bonding donor and acceptor, respectively).

Main water role	Hydrogen bond	D–H/Å	H···A/Å	D···A/Å	D–H···A/°
Coordinated to Cu1	O11W–H11A···O5 ⁱ	0.98	2.03	2.894(3)	146
	O11W–H11B···O13W ⁱ	1.01	2.21	3.009(4)	135
Coordinated to Cu2, Na2	O3W–H3A···O9W ⁱⁱ	0.99	1.89	2.812(1)	155
	O3W–H3B···O9W	0.98	1.88	2.845(1)	166
	O1W–H1A···O15W	0.99	1.84	2.772(2)	155
	O1W–H1B···O10 ⁱⁱⁱ	0.99	1.93	2.866(2)	157
Coordinated to Na1	O2W–H2B···O12 ^{iv}	0.99	2.65	3.437(2)	136
	O4W–H4A···O2 ⁱ	1.06	2.01	2.775(2)	127
	O4W–H4B···O8 ⁱⁱⁱ	0.98	2.36	3.040(2)	126
	O5W–H5B···O10v	0.99	2.02	2.785(3)	132
Coordinated to Na3	O6W–H6A···O4W ^{vii}	1.01	1.76	2.757(2)	169
	O6W–H6B···O15W ^{vii}	0.98	2.08	2.966(2)	149
	O7W–H7A···O11W ^{viii}	0.99	1.99	2.938(3)	159
	O7W–H7B···O5W ^v	0.97	1.83	2.791(3)	169
	O10W–H10A···O5 ⁱ	0.98	1.84	2.738(3)	151
Coordinated to Na4	O10W–H10B···O2W ^{vii}	1.06	2.52	3.426(3)	142
	O13W–H13A*···O12Wix	1.02	1.81	2.671(4)	140
	O13W–H13B*···O5	1.02	2.20	3.063(4)	140
	O8W–H8A···N2	0.99	1.94	2.794(1)	144
	O8W–H8B···O8 ⁱⁱⁱ	1.00	2.40	3.216(1)	138
Non-coordinated	O9W–H9A···O8W ^x	1.00	1.82	2.812(2)	171
	O12W–H12A···O2W	0.97	2.14	2.768(2)	121
	O12W–H12B···O1 ^x	1.04	2.07	2.865(2)	132

Symmetry codes: (i) = $1-x, \frac{1}{2}+y, 1-z$; (ii) = $-x, \frac{1}{2}+y, 2-z$; (iii) = $-x, -\frac{1}{2}+y, 2-z$; (iv) = $x, y, 1+z$; (v) = $-x, -\frac{1}{2}+y, 1-z$; (vi) = $-x, \frac{1}{2}+y, 1-z$; (vii) = $x, y, -1+z$; (viii) = $x, -1+y, z$; (ix) = $x, -1+y, -1+z$; (x) = $x, 1+y, z$. *Hydrogen bonds performed by the major 60% occupancy sites set (O13W, H13A, H13B) are listed (O14W, H14A, H14B in the minor 40% occupancy sites set exhibit the same hydrogen bonding pattern with slightly different metrics).

Table S5. Hydrogen bonds present in the crystal structure of **2** (D and A are abbreviations for hydrogen bonding donor and acceptor, respectively).

Hydrogen bond	D–H/Å	H···A/Å	D···A/Å	D–H···A/°
O1W–H1W···N2	0.86	2.14	2.919(7)	151
O1W–H2W···O3W ⁱ	1.00	2.03	2.858(8)	139
O2W–H3W···N5	0.86	2.03	2.859(8)	165
O2W–H4W···O1W	1.01	2.03	2.872(9)	139
O3W–H5W···O11	0.85	2.22	2.864(2)	133
O4W–H7W···O5	0.97	1.89	2.774(2)	150
O4W–H8W···O4	0.98	2.03	2.888(2)	146
O5W–H9W···O6	0.86	2.14	2.987(2)	168
O5W–H9W···O12	0.86	2.63	3.192(3)	124
O5W–H10W···O3W	0.99	2.54	3.220(2)	126

Symmetry code: (i) = $1-x, 1-y, 1-z$.

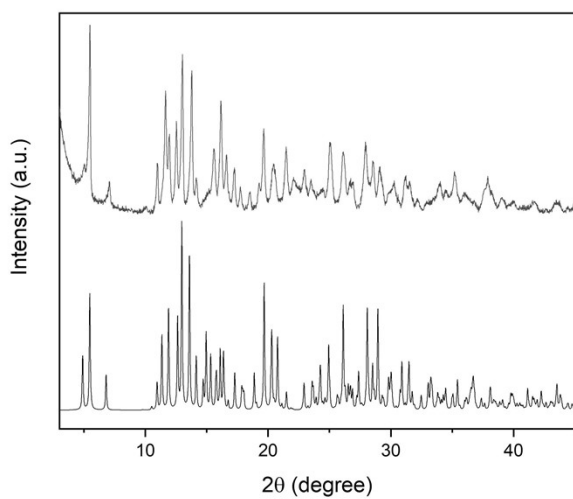


Figure S1. Experimental PXRD patterns of **1** (a, blue line) compared to the calculated ones (black lines).

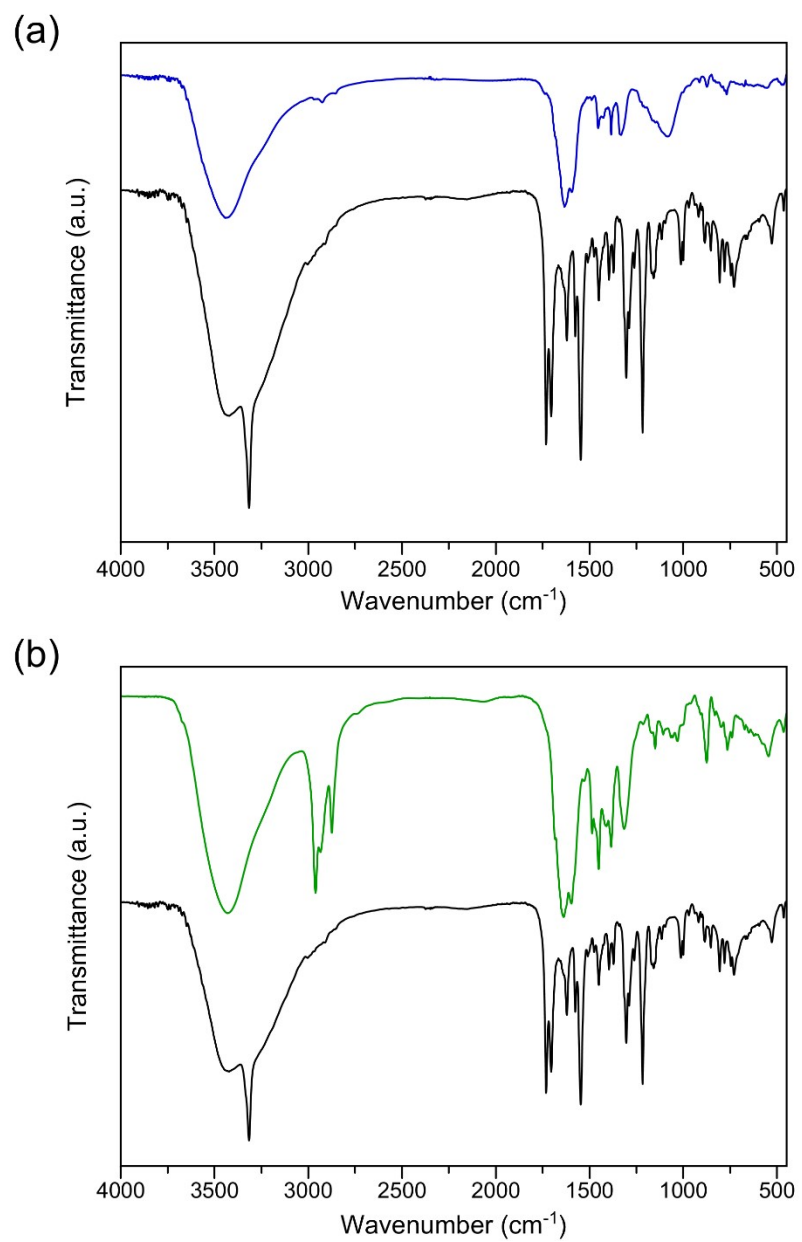


Figure S2. FT-IR spectra of **1** (a, blue line) and **2** (b, green line) compared to that of the $\text{H}_2\text{Et}_2\text{acriba}$ proligand (black lines).

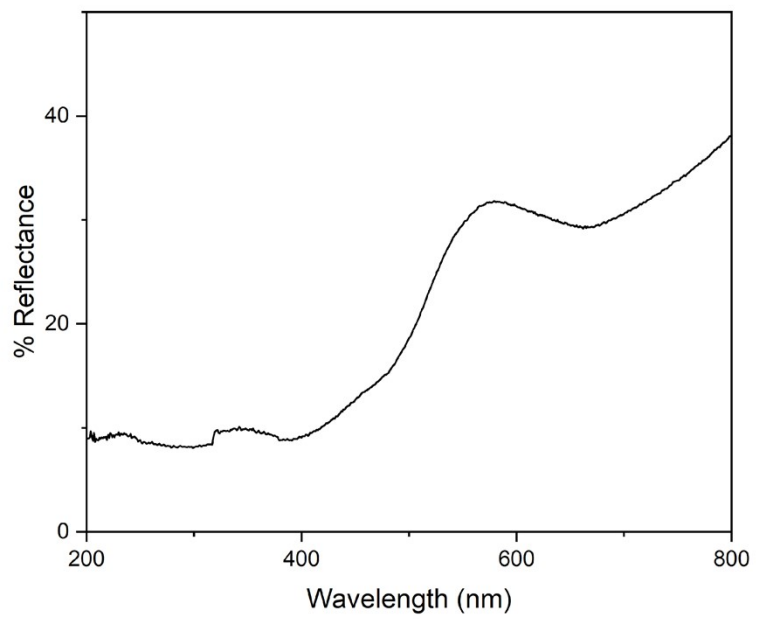


Figure S3. UV-Vis spectra of solid sample of **1**.

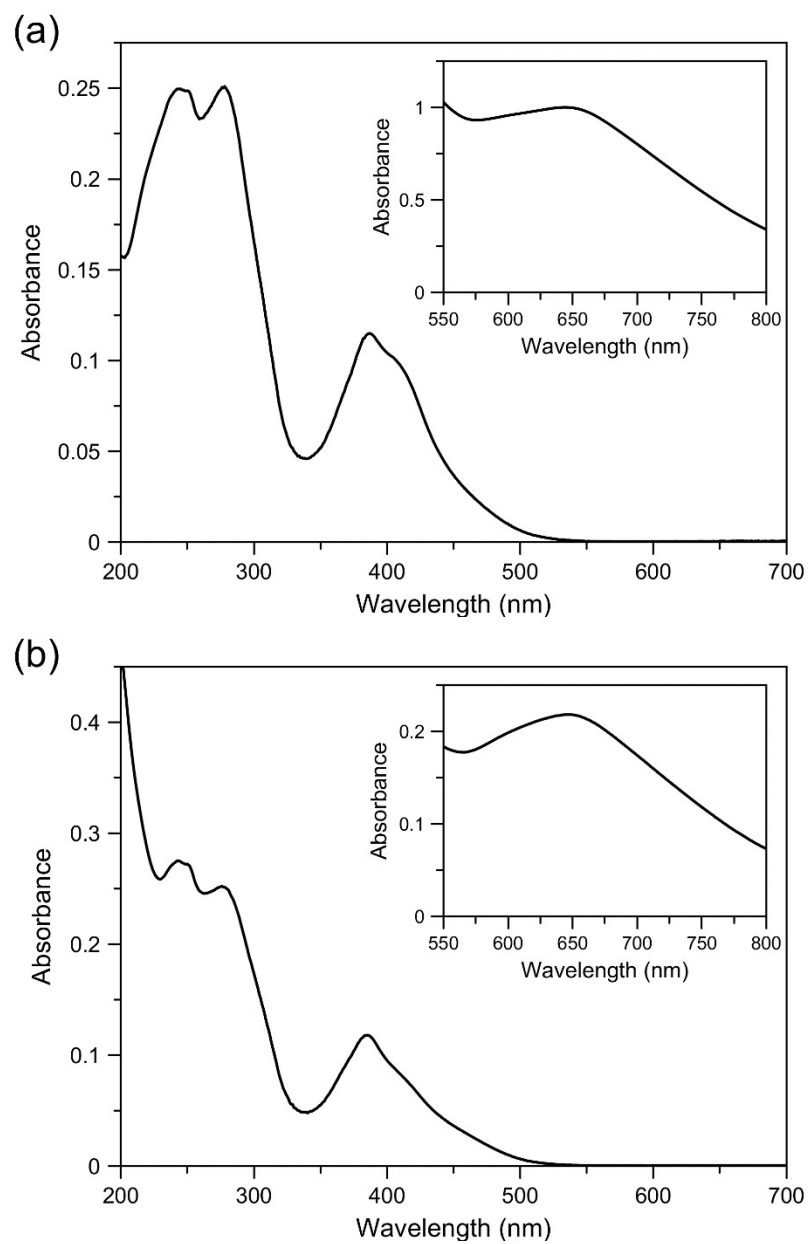


Figure S4. Electronic absorption spectra of **1** (a) and **2** (b) in aqueous solution ($[1] = 0.002 \mu\text{M}$, $[2] = 0.02 \mu\text{M}$). The inset shows the visible region for concentrated aqueous solutions ($[1] = 5.0 \text{ mM}$, $[2] = 1.0 \text{ mM}$).

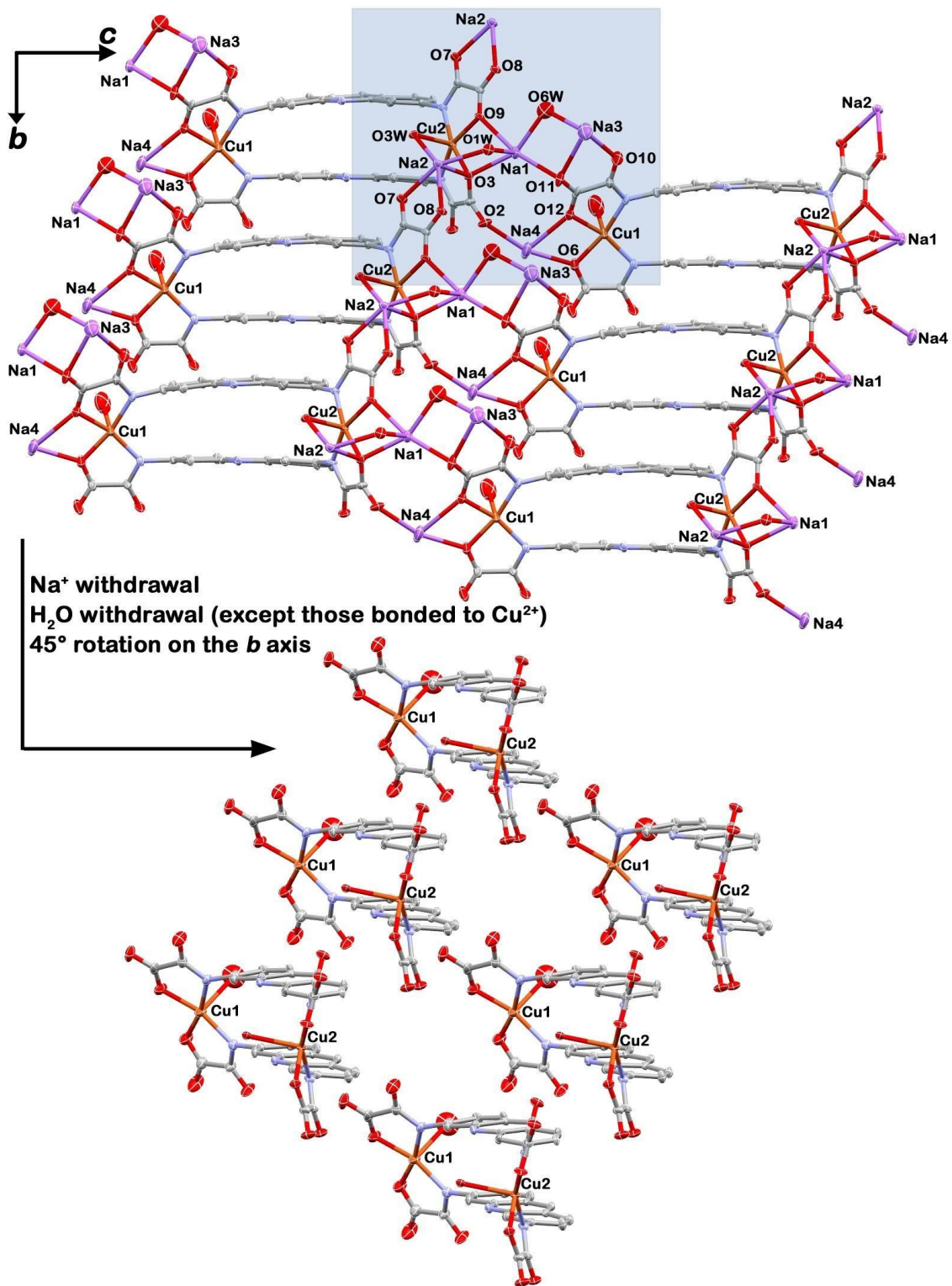


Figure S5. The connection of the dicopper(II) building blocks onto the (100) plane. Only the oxygens engaged in these cross-links are shown, which had their labels shown once in the framed area together with those of the metal ions (labelled in all picture). The ladder-like arrangement of the building blocks is illustrated at the bottom.

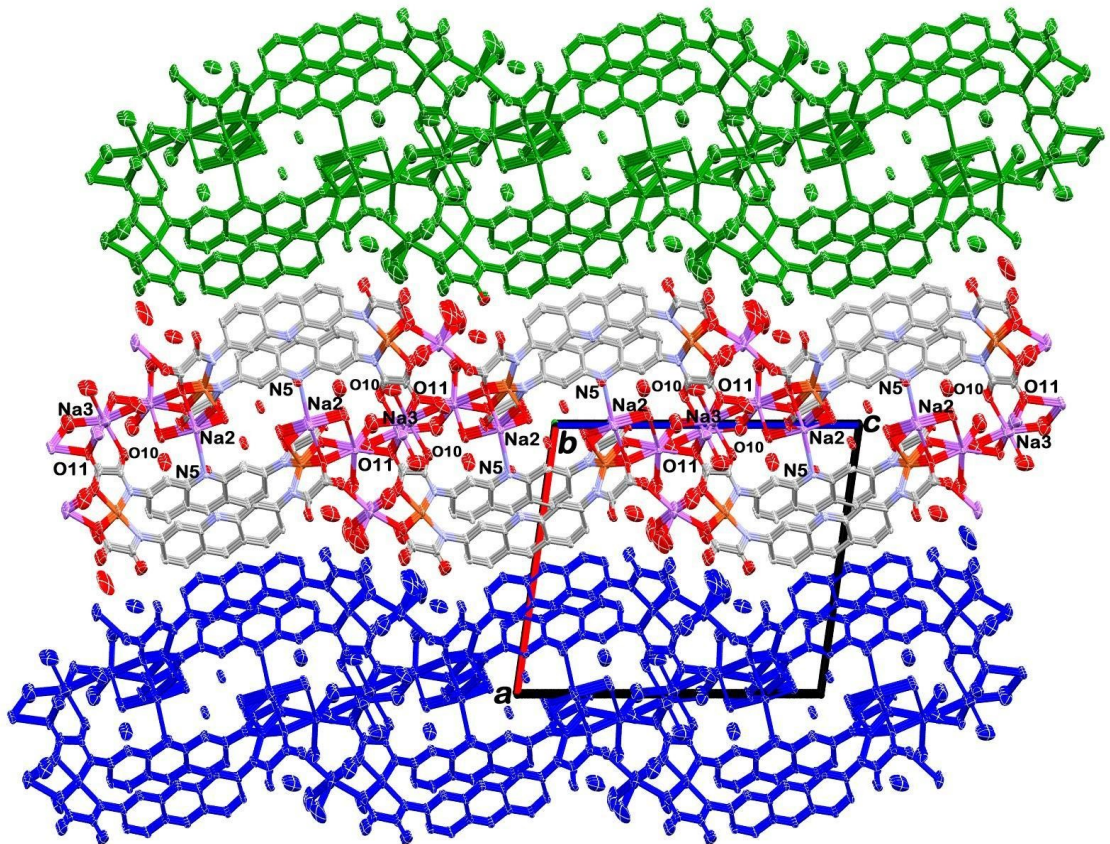


Figure S6. View of three layer fragments of **1** growing along the (100) plane (green, blue and atom-colored sheets). The labelled atoms stabilize the layers through the $\text{Na}_2\text{--N}5$, $\text{Na}_3\text{--O}10$ and $\text{Na}_3\text{--O}11$ coordination bonds, in addition to those bonds shown in Figure S5

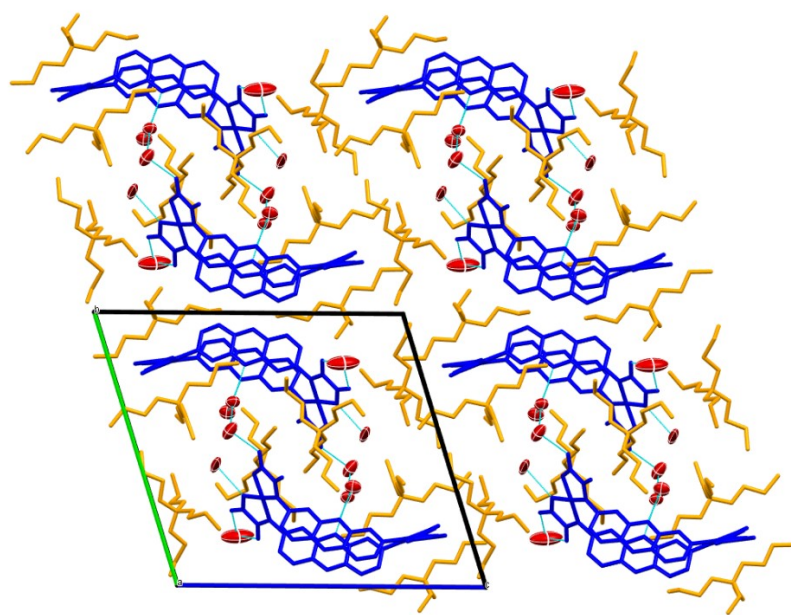


Figure S7. Perspective view of the crystal packing of **2** along the crystallographic *a* axis. The dicopper(II) metallacycophane anions, the tetrabutylammonium cations and the water molecules are shown in blue, orange and red, respectively. The hydrogen bonding network involving water molecules and oxamate oxygen atoms is represented as cyan lines.

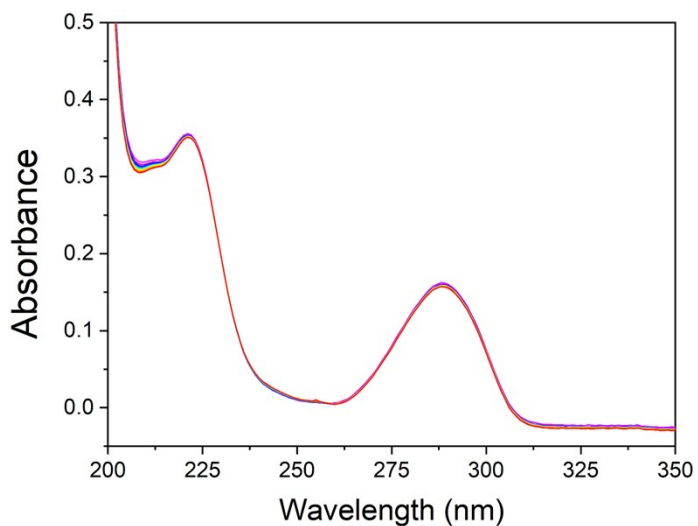


Figure S8. Evolution of electronic absorption spectra of the spontaneous oxidation of H₂Q at 25 °C during one hour. [H₂Q]₀ = 75 μmol L⁻¹.

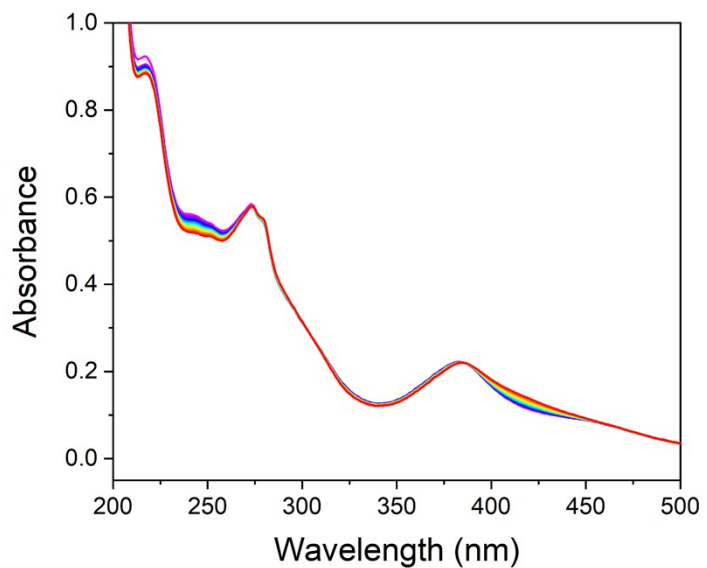
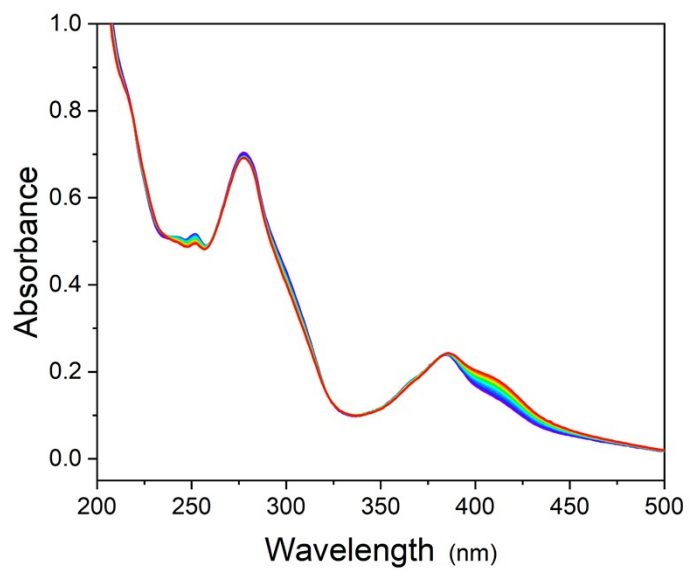


Figure S9. Evolution of electronic absorption spectra of the oxidation catechol (a) and resorcinol (b) catalyzed by **1** at 25 °C under O₂ saturation. [Phenolic derivative]₀ = 75 μmol L⁻¹ and [1] = 7.5 μmol L⁻¹.

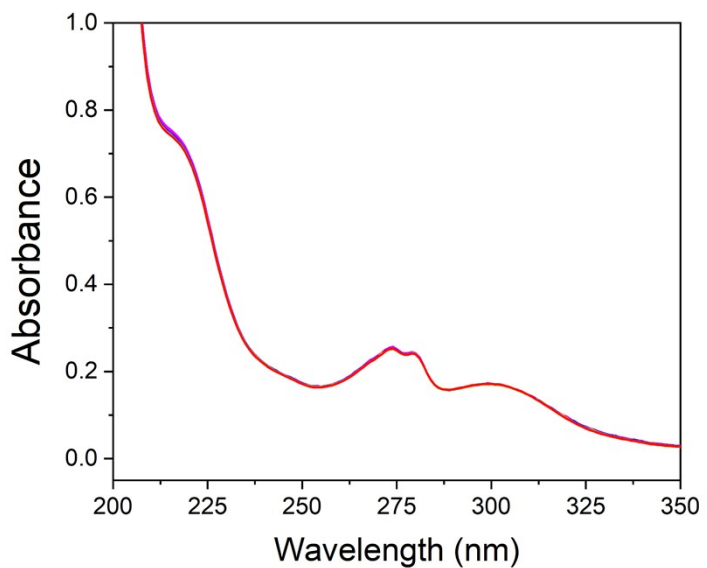
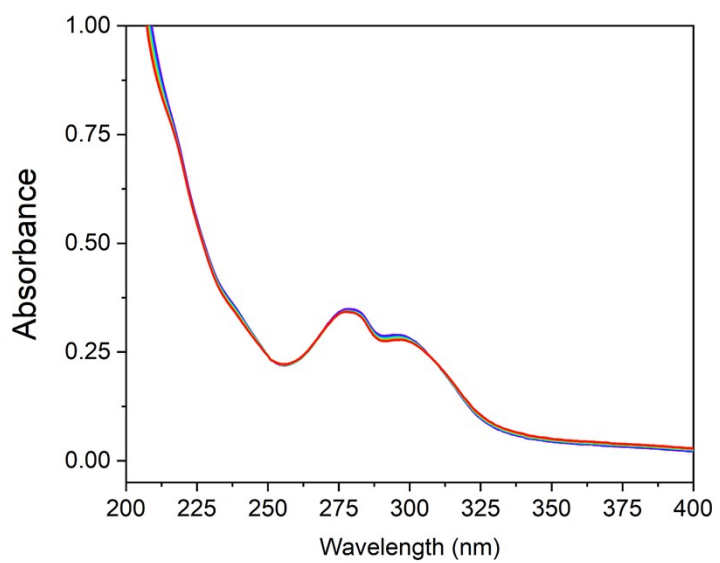


Figure S10. Evolution of electronic absorption spectra of the oxidation catechol (a) and resorcinol (b) catalyzed by **3** at 25 °C under O₂ saturation. [Phenolic derivative]₀ = 75 μmol L⁻¹ and [3] = 7.5 μmol L⁻¹.

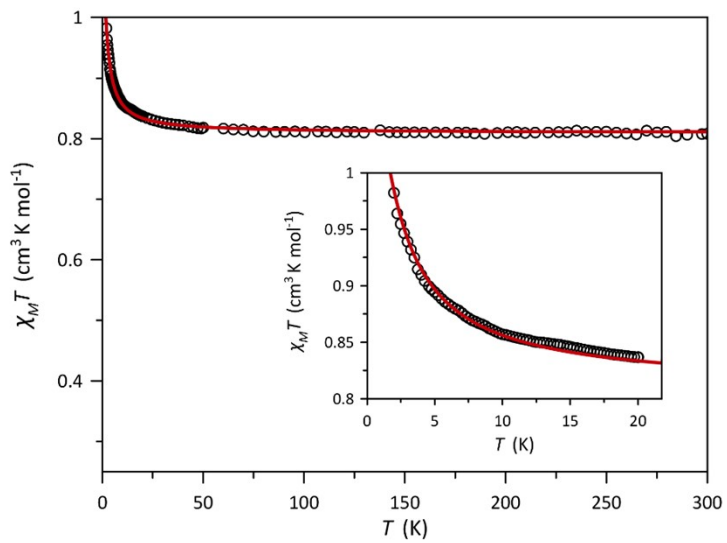


Figure S11. Thermal dependence of $\chi_M T$ for **2**: (empty circles) experimental; (solid line) best-fit curve through the Bleaney-Bowers equation. The inset shows a detail of the low-temperature region.

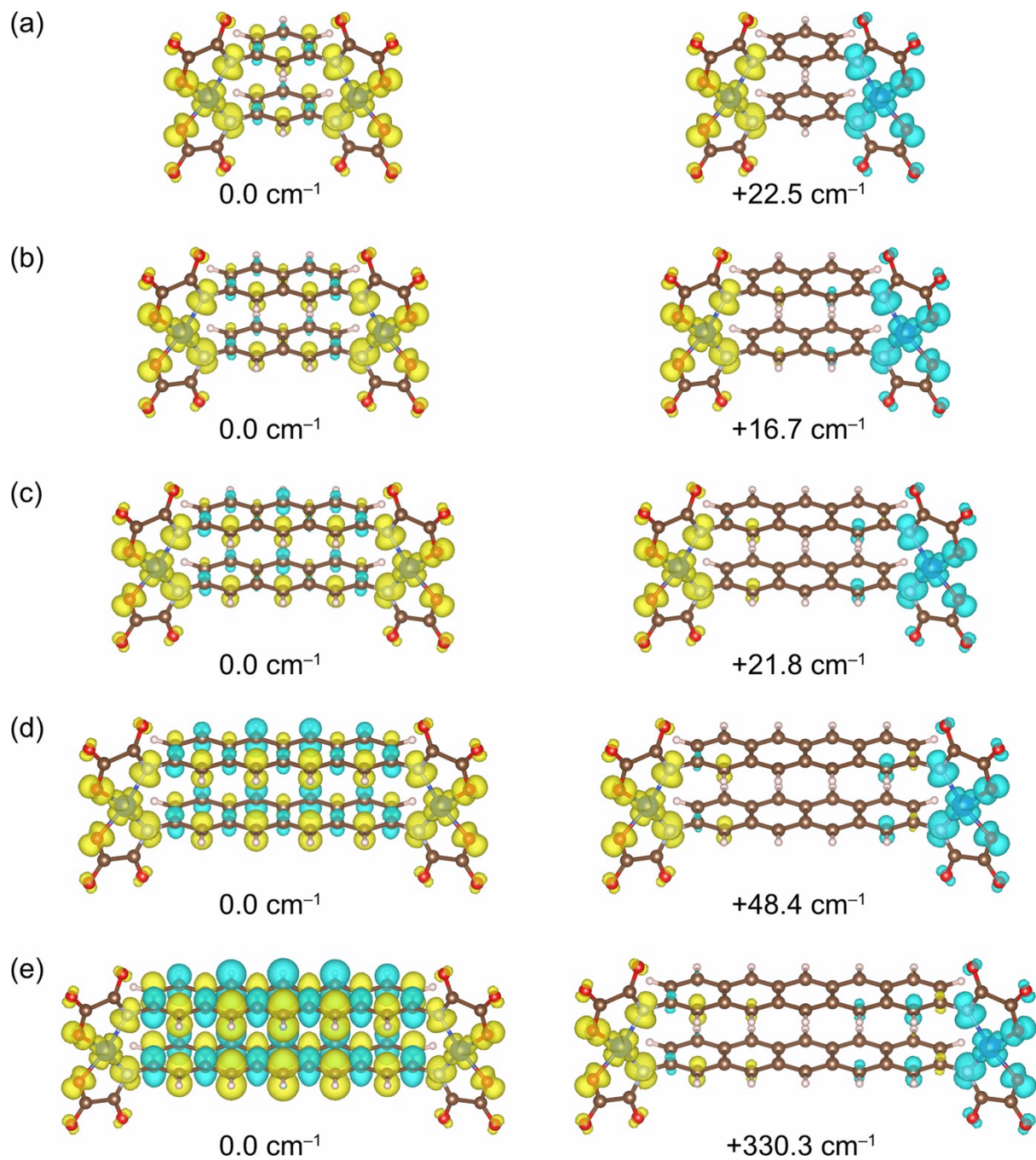


Figure S12. Calculated spin density maps for triplet (T, left) and singlet (S, right) states of dinuclear copper(II) models featuring oligoacene ($X = \text{CH}$ in Fig. 7) spacers of sizes $N = 1\text{--}5$ (a-e) in an idealized geometry (see text). Yellow and blue isodensity surfaces represent positive and negative spin densities with a cut-off value of $0.0018 \text{ e bohr}^{-3}$. The numerical values indicate of energy each state with respect to the triplet T (right).

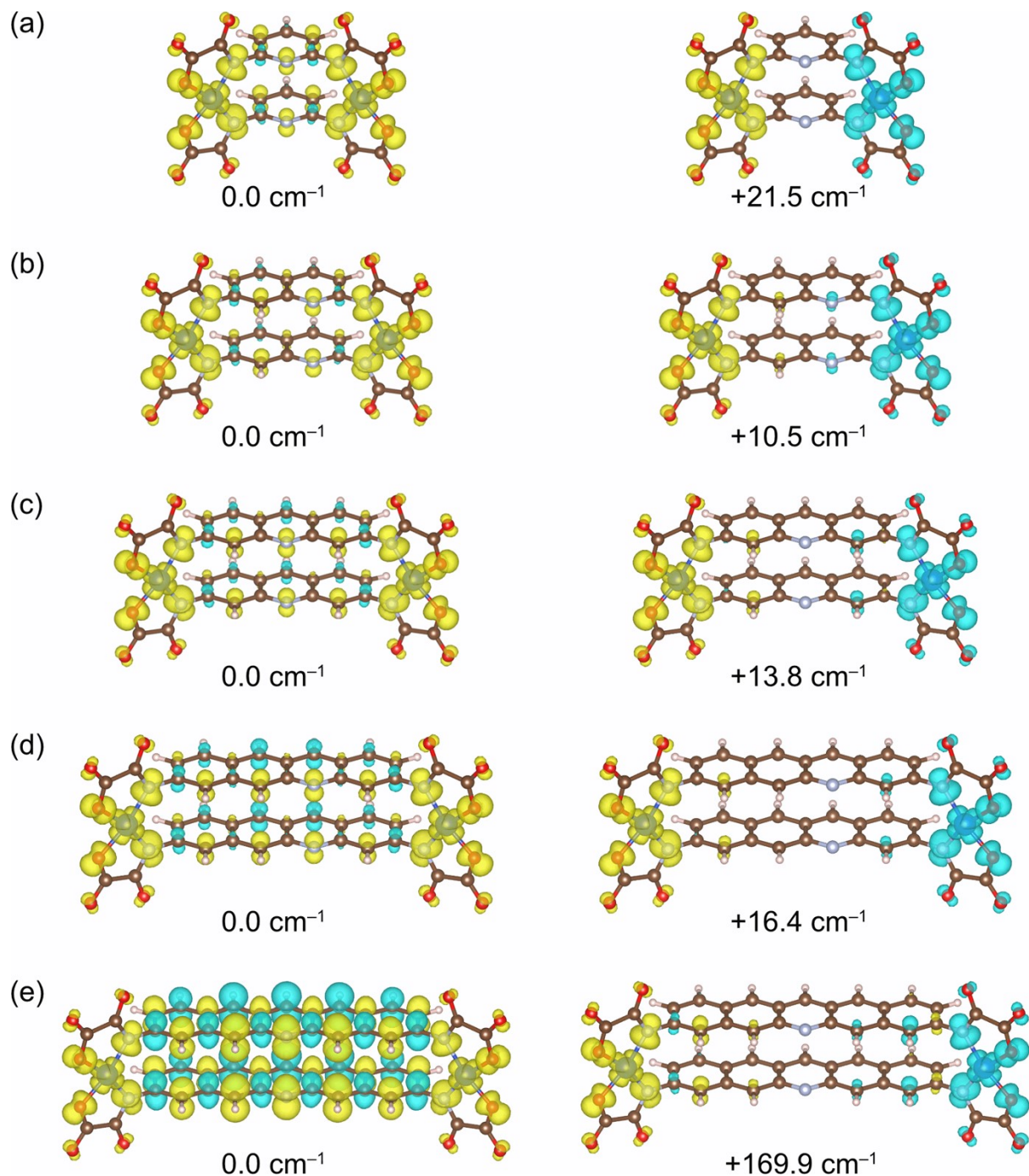


Figure S13. Calculated spin density maps for triplet (T, left) and singlet (S, right) states of dinuclear copper(II) models featuring pyridine-oligoacene ($X = N$ in Fig. 7) spacers of sizes $N = 1-5$ (a-e) in an idealized geometry (see text). Yellow and blue isodensity surfaces represent positive and negative spin densities with a cut-off value of $0.0018 \text{ e bohr}^{-3}$. The numerical values indicate of energy each state with respect to the triplet T (right).

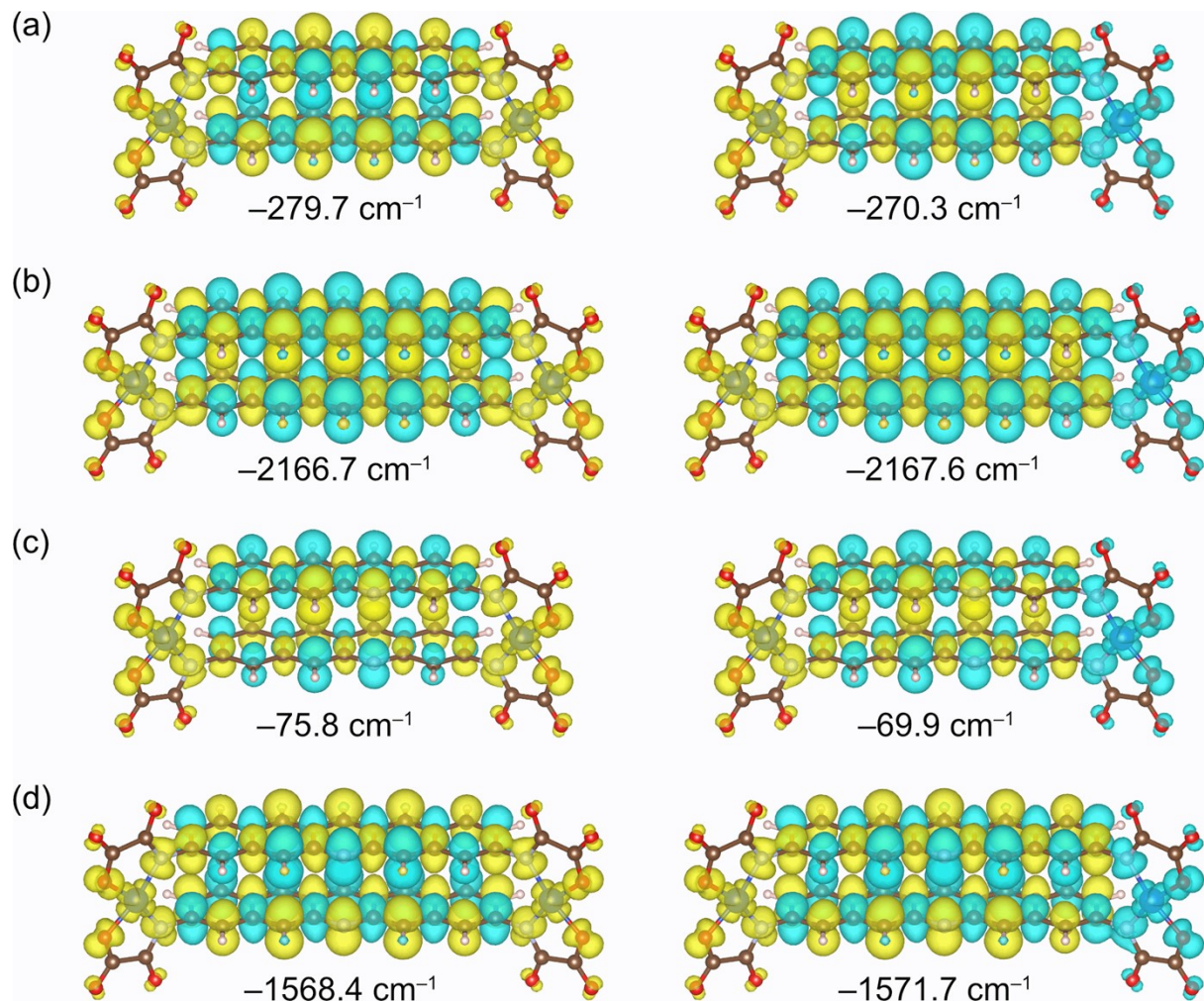


Figure S14. Calculated spin density maps for most stable triplet (T' , left) and singlet (S' , right) states of dinuclear copper(II) models featuring oligoacene ($X = \text{CH}$, a-b) and pyridine-oligoacene ($X = \text{N}$, c-d) spacers (see Fig. 7) of sizes $N = 4$ (a and c) and 5 (b and d) in an idealized geometry (see text). Yellow and blue isodensity surfaces represent positive and negative spin densities with a cut-off value of $0.0018 \text{ e bohr}^{-3}$. The numerical values indicate of energy each state with respect to the triplet T (right, see Figs. S15 and S16).

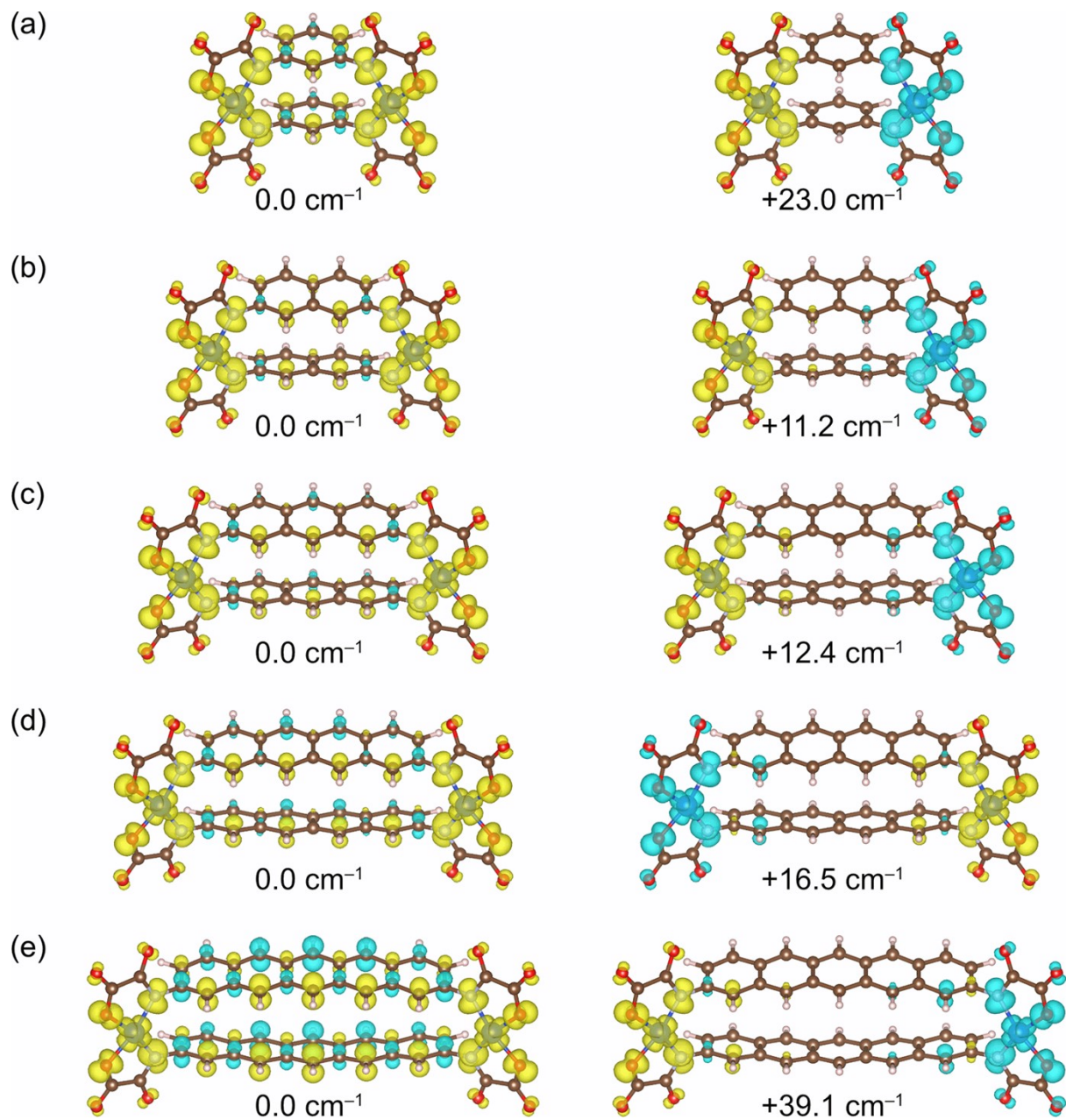


Figure S15. Calculated spin density maps for triplet (T, left) and singlet (S, right) states of dinuclear copper(II) models featuring oligoacene ($X = \text{CH}$ in Fig. 7) spacers of sizes $N = 1-5$ (a-e) in an optimized geometry (see text). Yellow and blue isodensity surfaces represent positive and negative spin densities with a cut-off value of $0.0018 \text{ e bohr}^{-3}$. The numerical values indicate of energy each state with respect to the triplet T (right).

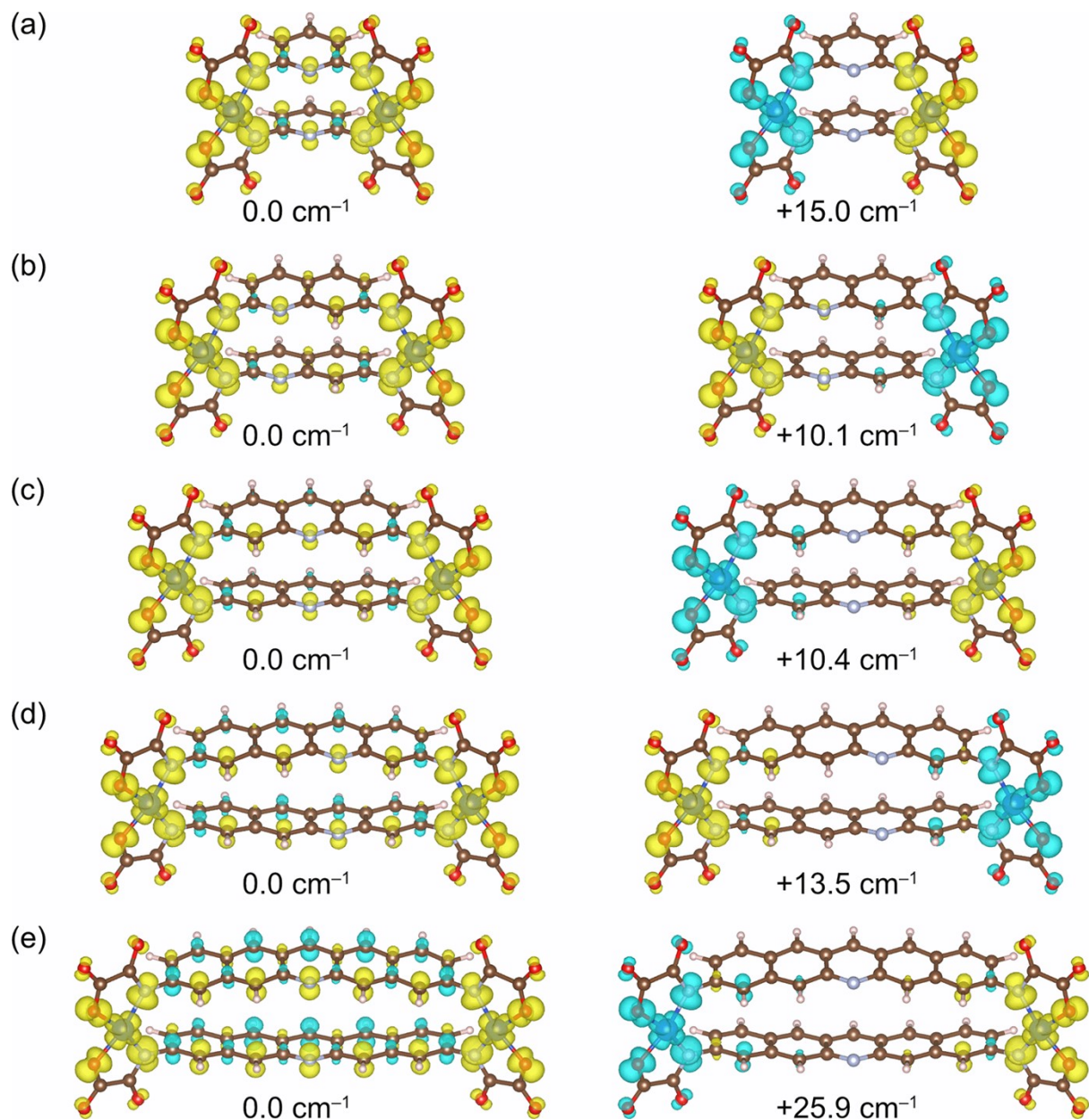


Figure S16. Calculated spin density maps for triplet (T, left) and singlet (S, right) states of dinuclear copper(II) models featuring pyridine-oligoacene ($X = N$ in Fig.7) spacers of sizes $N = 1\text{--}5$ (a-e) in an optimized geometry (see text). Yellow and blue isodensity surfaces represent positive and negative spin densities with a cut-off value of $0.0018 \text{ e bohr}^{-3}$. The numerical values indicate of energy each state with respect to the triplet T (right).